Applied Catalysis B: Environmental 182 (2016) 85–93

Contents lists available at ScienceDirect

Applied Catalysis B: Environmental

journal homepage: www.elsevier.com/locate/apcatb

The selective deposition of silver nanoparticles onto {1 0 1} facets of TiO_2 nanocrystals with co-exposed {0 0 1}/{1 0 1} facets, and their enhanced photocatalytic reduction of aqueous nitrate under simulated solar illumination

Dechen Sun[a,1], Weiyi Yang[a,1], Long Zhou[a], Wuzhu Sun[a], Qi Li[a,*], Jian Ku Shang[b]

[a] Environment Functional Materials Division, Shenyang National Laboratory for Materials Science, Institute of Metal Research, Chinese Academy of Sciences, Shenyang 110016, PR China
[b] Department of Materials Science and Engineering, University of Illinois at Urbana-Champaign, Urbana, IL 61801, USA

ARTICLE INFO

Article history:
Received 4 June 2015
Received in revised form 1 September 2015
Accepted 2 September 2015
Available online 8 September 2015

Keywords:
Photocatalytic reduction
TiO_2 nanocrystals with co-exposed {0 0 1}/{1 0 1} facets
Selective deposition of Ag nanoparticles
Aqueous nitrate removal
Solar illumination

ABSTRACT

Highly efficient photocatalytic reduction of environmental pollutants requires the enrichment of photogenerated electrons on the photocatalyst's surface. Thus, proper material design and modification are needed to efficiently separate photogenerated electron/hole pairs and achieve their oriented migrations for the enrichment of photogenerated electrons on their surface. In this work, a modified photodeposition process was developed which successfully deposited silver nanoparticles selectively on {1 0 1} facets of TiO_2 nanocrystals with co-exposed {0 0 1}/{1 0 1} facets. The synergistic effect of crystal facet engineering and the selective deposition of silver nanoparticles on {1 0 1} facets largely enhanced the separation of photogenerated carriers and enriched the presence of photo-generated electrons onto the surface of TiO_2 to a net negative-charged surface. A strong photocatalytic reduction capability of the sample was demonstrated by its superior photocatalytic reduction activity on aqueous nitrate under a simulated solar illumination. The removal ratio of aqueous nitrate reached ~95%, and most of the reduction product was the desirable N_2 with the selectivity over 90%. These TiO_2 nanocrystal with co-exposed {0 0 1}/{1 0 1} facets and silver modification on {1 0 1} facets could also effectively remove both nitrate and various organic pollutants from water simultaneously.

1. Introduction

Titanium dioxide (TiO_2) is one of the most important semiconductor-based photocatalysts and had been widely studied for both solar energy conversion and environmental applications [1–3]. For its environment applications, most studies focused on the photocatalytic oxidation of various environmental pollutants, while the studies on the photocatalytic reduction of environmental pollutants were relatively limited. When TiO_2 is excited, both electron and hole are produced, and photocatalytic reactions happen when photogenerated electrons and holes migrate to its surface and react with substances absorbed on/near its surface. For the photocatalytic reduction of environmental pollutants, they react with photogenerated electrons [4–6]. Thus, in order to enhance the photocatalytic reduction activity of TiO_2, proper material design and modification are needed to efficiently separate photogenerated electron/hole pairs and achieve their oriented migrations to enrich the presence of photogenerated electrons on the surface of TiO_2.

Since the pioneering report by Yang et al. on the synthesis of anatase TiO_2 sheets with 47% exposed {0 0 1} facets in 2008 [7], crystal facet engineering is becoming an important approach to obtain photocatalysts with higher activity [8–13]. Recently, anatase TiO_2 nanocrystals with exposed facets were developed, which demonstrated enhanced photocatalytic performance than their counterparts in the micrometer size range due to their largely increased surface areas [14–18]. It was found that the photocatalytic activity of anatase TiO_2 could be further modulated by incorporating different exposed crystal facets [19–22]. Because there are slight surface energy differences of the valence and conduction bands between different facets, photogenerated electrons and holes could be driven to different facets [23]. So the separation

* Corresponding author at: 72 Wenhua Road, Shenyang, Liaoning Province, 110016, PR China. Fax: +86 24 23971215.
E-mail addresses: qiliuiuc@gmail.com, qili@imr.ac.cn (Q. Li).
[1] These authors contributed equally to this work.

http://dx.doi.org/10.1016/j.apcatb.2015.09.005
0926-3373/

of photogenerated electrons and holes could be more effective and oriented in space, which could offer great opportunity for the selective photo-deposition of co-catalysts on designated facets. Both theoretical and experimental studies had demonstrated that there are more hole trapping centers on {0 0 1} facets of anatase TiO_2, while more electron trapping centers existed on {1 0 1} facets of anatase TiO_2 [24–26]. Thus, the high-energy {0 0 1} facets prefer to provide oxidation sites, while the low-energy {1 0 1} facets prefer to provide reduction sites [27–29].

Noble metal (Au, Pt, Ag etc.) modification is another effective way to initiate the oriented migration of photogenerated electrons due to their higher work functions compared with that of TiO_2 [30]. Noble metal nanoparticles deposited on the surface of TiO_2 could serve as trapping centers for photogenerated electrons and subsequently as active centers for photocatalytic reactions [31–33]. Thus, it would be desirable to selectively deposit noble metal nanoparticles onto {1 0 1} facets of anatase TiO_2 nanocrystals with co-exposed {0 0 1} and {1 0 1} facets, which could combine the advantages from both the crystal facet effect and noble metal modification to initiate the oriented migration of photogenerated electrons and further enrich their presence onto the surface of TiO_2 for the enhanced photocatalytic reduction activity. Although limited reports were available on the selective deposition of noble metals onto anatase TiO_2 with exposed facets [34–36], few studies had been conducted on the photocatalytic reduction activity of TiO_2 with noble metal modifications on selected facets.

Various processes had been developed to synthesize noble metal-modified TiO_2, including conventional impregnation method, sol–gel process, chemical deposition, and photo-deposition [37–39]. However, most of these processes were not feasible to generate noble metal nanoparticles of small and uniform size and the self-nucleation/crystal growth of noble metals in liquid phase was commonly found, which could be attributed to their relatively fast nucleation/crystal growth rates [40–42]. Herein, we reported a newly developed process to selectively deposit silver nanoparticles onto {1 0 1} facets of anatase TiO_2 nanocrystals with co-exposed {0 0 1}/{1 0 1} facets through a modified photo-deposition process. The synergistic effect of crystal facet engineering and the selective deposition of silver nanoparticles on {1 0 1} facets largely enhanced the separation of photogenerated carriers and enriched the presence of photogenerated electrons onto the surface of TiO_2 to a net negative-charged surface, which largely enhanced its photocatalytic reduction performance. As one of the most common groundwater contaminants, nitrate could cause various health problems to human beings and has a large impact on the natural nitrogen cycle [43–45]. These TiO_2 nanocrystal with co-exposed {0 0 1}/{1 0 1} facets and silver modification on {101} facets demonstrated a superior photocatalytic reduction activity on aqueous nitrate under a simulated solar illumination. The removal ratio of aqueous nitrate reached ~95%, and most of the reduction product was the desirable N_2 with the selectivity over 90%.

2. Experimental

2.1. Chemicals and material

Titanium (IV) fluoride (TiF_4; 98%, Shanghai Darui Chemicals Co., Ltd., Shanghai, PR China) was used in this study as the precursor to provide both titanium and fluorine sources. Tert-butanol ($C_4H_{10}O$; ≥98%, Sinopharm Chemical Reagent Co., Ltd., Shanghai, PR China) was used as the solvent in the solvent-thermal process. Commercially available Degussa P25 TiO_2 nanoparticles (Evonik Industries, Essen, Germany) were used as the TiO_2 standard for comparison purpose. Silver nitrate ($AgNO_3$; ≥99%, Sinopharm Chemical Reagent Co., Ltd., Shanghai, PR China) was used to provide the silver source in the photo-deposition process. Ethyl alcohol (C_2H_5OH; ≥99%, Sinopharm Chemical Reagent Co., Ltd., Shanghai, PR China) was used as the solvent in the photo-deposition process. Potassium nitrate (KNO_3; AR, Sinopharm Chemical Reagent Co., Ltd., Shanghai, PR China) and deionized (DI) water were used to prepare the stock solution of NO_3^-. Formic acid (HCOOH, AR, Sinopharm Chemical Reagent Co., Ltd., Shanghai, PR China) was used as the sacrificial agent in the photocatalytic nitrate reduction process. Glucose ($C_6H_{12}O_6$, AR, Sinopharm Chemical Reagent Co., Ltd., Shanghai, PR China), ammonium hydroxide($NH_3{\cdot}H_2O$, 28%, Sinopharm Chemical Reagent Co., Ltd., Shanghai, PR China) were used to deposit silver nanoparticles on TiO_2 nanocrystals by the chemical reduction process. Model organic pollutants, including humic acid sodium salt (Sinopharm Chemical Reagent Co., Ltd., Shanghai, PR China), orange II sodium salt (AO7, $C_{16}H_{11}N_2NaO_4S$, AR, Sinopharm Chemical Reagent Co., Ltd., Shanghai, PR China), and benzene (C_6H_6, AR, Sinopharm Chemical Reagent Co., Ltd., Shanghai, PR China), were also used as sacrificial agents in the photocatalytic nitrate reduction experiment.

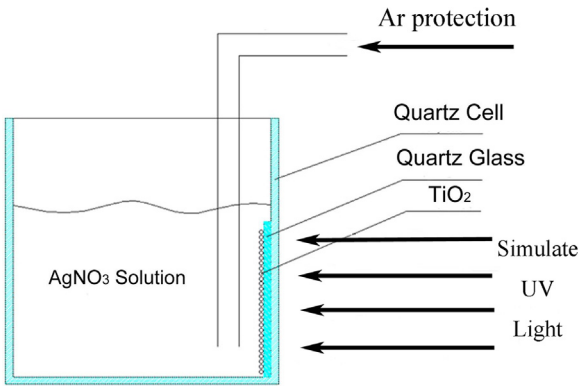

Fig. 1. The schematic illustration of the selective photo-deposition reactor set-up for depositing silver nanoparticles on TiO_2 nanocrystals with co-exposed {0 0 1}/{1 0 1} facets.

2.2. Synthesis of TiO_2 nanocrystal with co-exposed {0 0 1}/{1 0 1} facets and silver-modification on {1 0 1} facet

In a typical synthesis process [17], 1.6 g of TiF_4 was dissolved in 400 mL of tert-butanol under continuous stirring to obtain a transparent faint yellow solution. Then, the solution was transferred to an autoclave and allowed to alcoholize at 160 °C for 72 h. The precipitated powders were filtered, washed with ethyl alcohol to remove residual solvent for three times, and then dried at 50 °C overnight to obtain the as-prepared TiO_2 nanocrystals with co-exposed {0 0 1}/{1 0 1} facets.

The selective deposition of silver nanoparticles onto {1 0 1} facets of these TiO_2 nanocrystals with co-exposed {0 0 1}/{1 0 1} facets was conducted by a modified photo-deposition process we developed. 50 mg TiO_2 nanocrystals with co-exposed {0 0 1}/{1 0 1} facets were dispersed in 5 mL ethyl alcohol by ultrasonic dispersion. A quartz plate was cleaned with DI water and ethyl alcohol for several times, dried with the argon purging, and then used as the substrate for spin coating (TC-218, Shenyang Sile Machinery Manufacturing Co., Ltd., PR China). The rotate speed was fixed at 1500 r/min, and 1 mL TiO_2 suspension was slowly dropped onto the quartz plate surface to generate a uniform TiO_2 thin film on it. Finally, the quartz plate was dried at 50 °C for 8 h to enhance the adhesion of TiO_2 thin film before it was used for the selective photo-deposition experiment.

Fig. 1 schematically demonstrates the selective photo-deposition experiment set up. The quartz plate coated with TiO_2 thin film was first illuminated by UV light ($\lambda < 420$ nm, 10 mW/cm^2) for 10 min to activate the oxidative {0 0 1} facets and the reductive {1 0 1} facets. Then it was fixed on the side of a 100 mL quartz groove, in which 50 mL ethanol solution of silver nitrate (10^{-4} M) was already purged with argon for 30 min to remove dissolved oxygen. Next, UV light was switched on for 5 min, which illuminated the quartz plate and TiO_2 thin film first before it reached the $AgNO_3$ solution under argon atmosphere. After the illumination, the quartz plate was softly rinsed with DI water first and then ultrasonically cleaned for 30 min to remove TiO_2 thin film from the quartz plate, and the obtained precipitates were washed with DI water for several times and then dried at 50 °C for 8 h to obtain TiO_2 nanocrystals with co-exposed {0 0 1}/{1 0 1} facets and silver nanoparticle modification on {1 0 1} facets, which was denoted as Ag/TiO_2 (Photo).

For comparison purpose, two other samples were also prepared in this study. The same modified photo-deposition process was conducted on Degussa P25 TiO_2 nanoparticles and the obtained sample was denoted as Ag/P25 (Photo). The other sample was prepared by the chemical reduction method, in which 50 mg of TiO_2 nanocrystals with co-exposed {0 0 1}/{1 0 1} facets were dispersed in 50 mL silver-ammonia solution (Ag:Ti = 1:200) by ultrasonic dispersion and then kept stirring magnetically for 30 min. Then, 10 mL glucose solution ($n(Ag^+)$: $n(C_6H_{12}O_6) = 1:10$) was added into the suspension, and the suspension was kept stirring magnetically for another 30 min. The obtained precipitates were washed with DI water and dried at 50 °C for 8 h to obtain silver modified TiO_2 nanocrystals with co-exposed {0 0 1}/{1 0 1} facets, which was denoted as Ag/TiO_2 (Chem).

2.3. Characterization

X-ray diffraction (XRD) experiments were conducted on a D/MAX-2004 X-ray powder diffractometer (Rigaku Corporation, Tokyo, Japan) with Ni-filtered Cu Kα ($\lambda = 0.15418$ nm) radiation at 56 kV and 182 mA to analyze the crystal structure and crystallite size of obtained samples. Their morphologies were examined by transmission electron microscopy (TEM) on a JEOL 2100 TEM (JEOL Ltd., Tokyo, Japan) operated at 200 kV, with a point-to-point resolution of 0.28 nm. TEM samples were prepared by dispersing a thin film of these powder samples on Cu grids. X-ray photoelectron spectroscopy (XPS) measurements were made using an ESCALAB250 X-ray photoelectron spectrometer (Thermo Fisher Scientific Inc., Waltham, MA, USA) with an Al Kα anode (1486.6 eV photon energy, 300W). The UV–vis spectra of these samples were measured on a UV-2550 spectrophotometer (Shimadzu Corporation, Kyoto, Japan). The surface photovoltage spectra (SPS) of samples were measured with a home-built apparatus that had been described in details elsewhere [46].

2.4. Photocatalytic reduction of nitrate under simulated solar illumination

All photocatalytic removal of aqueous nitrate experiments were conducted at ~25 °C in 250 mL airtight glass containers. A 300 W xenon lamp (PLS-SXE300, Beijing Perfect Light Technology Co. Ltd., Beijing, China) was used as the light source, which provided light illumination similar to solar illumination (see Fig. S1 in the Supplementary material). A cooling water bath was used to minimize the temperature increase in nitrate solution under the light illumination. For each experiment, 100 mL KNO_3 solution with the initial aqueous nitrate concentrations of ~100 mg/L was used, the photocatalyst dosage was fixed at 0.5 g/L, the molecular ratio of sacrificial HCOOH to NO_3^- was ~5:1, the light intensity was ~30 mW/cm^2, and the illumination time was up to 3 h. Photocatalyst samples were dispersed in KNO_3 solution ultrasonically and the suspension was then magnetically stirred during the photocatalytic experiment to ensure a good contact between photocatalysts and NO_3^-. For the concentration analysis of remaining NO_3^- and photocatalytic reaction products of NO_2^- and NH_4^+, certain amount of the treated solution was collected regularly and then centrifuged at 12,000 rpm to recover photocatalysts and obtain the supernatant solution. The concentrations of NO_3^-, NO_2^- and NH_4^+ in the supernatant solution were analyzed by an ion chromatograph (Dionex ICS 1100 Ion Chromatography, Thermal Scientific, Sunnyvale, CA, U.S.A.).

Three commonly found organic pollutants in ground water were also used as sacrificial agents in the photocatalytic reduction of aqueous nitrate under simulated solar illumination by the Ag/TiO_2 (photo) sample, respectively, to examine its multifunctional capability to effectively remove both nitrate and organic pollutants from water simultaneously. The initial concentration of humic acids, AO7 dye, and benzene were ~50 mg/L, 20 mg/L, and 10 mg/L, respectively, and the nitrate concentration was ~100 mg/L. Other experimental conditions were the same as that with HCOOH as the sacrificial agent. The remaining concentrations of humic acids, AO7 dye, and benzene were determined by a UV–vis Spectrophotometer (JASCO-550, Shimadzu Corporation, Kyoto, Japan).

3. Results and discussion

3.1. Deposition of Ag nanoparticles on {1 0 1} facets of TiO_2 nanocrystals with co-exposed {0 0 1}/{1 0 1} facets

Fig. 2a shows the XRD pattern of the as prepared TiO_2 sample by the solvent-thermal process. All XRD peaks belonged to anatase TiO_2 (JCPDS No. 21-1272; space group: I41/amd (141)), and no rutile phase observed. Fig. 2b shows the HRTEM image of the as-prepared TiO_2 sample. It clearly demonstrated that these nanocrystals were well-faceted. Two sets of atomic planes with lattice spacing of 0.235 nm and 0.352 nm were observed, which corresponded to the (0 0 1) and (1 0 1) lattice planes of anatase TiO_2, respectively. From the HRTEM observation, {0 0 1} lattice planes were parallel to the top and bottom planes of the as-prepared TiO_2 nanocrystals, while {1 0 1} lattice planes were parallel to the eight sides of the as-prepared TiO_2 nanocrystals. Thus, {0 0 1} and {1 0 1} facets were co-exposed in the as-prepared TiO_2 nanocrystals. From TEM observation and the symmetry of anatase TiO_2 nanocrystals, the geometry of the as-prepared TiO_2 nanocrystals could be schematically described as the insert of Fig. 2b. Their side length was ~20–40 nm, and their thickness was ~6–10 nm. From their size and geometry, the percentages of exposed facets in the as-prepared TiO_2 nanocrystals were calculated on 20 TiO_2 nanocrystals by the method developed by Zhu et al. [17]. The average percentage of {0 0 1} facet was ~60%, while that of {1 0 1} facet was ~40%.

Fig. 3a shows the XRD pattern of the Ag/TiO_2 (photo) nanocrystals after the selective deposition of silver nanoparticles onto the as prepared TiO_2 nanocrystals by the modified photo-deposition process we developed. No obvious Ag XRD peaks could be clearly identified, which could be attributed to the low Ag loading amount and/or the fine size of Ag nanoparticles. Fig. 3b shows the representative HRTEM image of the Ag/TiO_2 (photo) sample. It demonstrated that very fine nanoparticles (3–6 nm) were only deposited on the {1 0 1} facets of these TiO_2 nanocrystals. The insert of Fig. 3b shows the HRTEM image of a small nanoparticle deposited on the {1 0 1} facet of one TiO_2 nanocrystal. Atomic planes with a lattice spacing of 0.242 nm could be easily observed, which corresponded to Ag (1 0 1) facets (JCPDS No. 04-0783; space group: Fm3m (225)). A large number of HRTEM images were examined on samples prepared in different batches, no Ag nanoparticle deposition happened

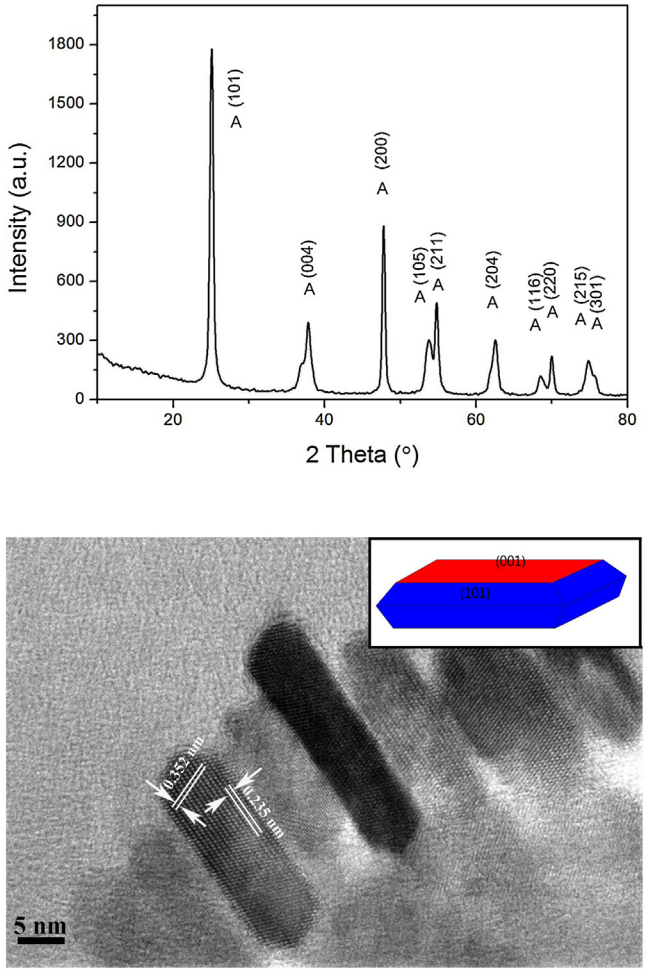

Fig. 2. (a) XRD pattern and (b) HRTEM image of as-prepared TiO_2 nanocrystals with co-exposed {0 0 1}/{1 0 1} facets. (Note: Insert plot in Fig. 2B shows the schematic illustration of the geometry of as-prepared TiO_2 nanocrystals).

on {0 0 1} facets of TiO_2 and no Ag nanoparticles existed by themselves. A TEM image of the Ag/TiO_2 (photo) sample with lower magnification could be found in Fig. S2a in the Supplementary material, which showed Ag nanoparticles on {1 0 1} facets of different TiO_2 nanocrystals.

XPS analysis was further conducted to verify the existence of Ag modification in our sample. Fig. 3c shows a representative XPS survey spectrum of the Ag/TiO_2 (photo) sample, which clearly demonstrated the existence of Ti, O, Ag, and C in the sample. Fig. 3d shows the high resolution XPS scan over Ag 3*d* peak region. It demonstrated clearly that two Ag 3*d* peaks (centered at 367.99 eV and 374 eV, respectively) with the peak position difference of ~6 eV existed, which corresponded to Ag^0 [47]. Thus, XPS analysis further confirmed that the deposited nanoparticles on the {1 0 1} faces of our sample were metallic Ag. The amount of Ag nanoparticles in the Ag/TiO_2 (photo) sample was measured by the inductively coupled plasma–mass spectrometry (ICP–MS), and Ag:Ti molar ratio was determined at ~1:200.

For comparison purpose, the Ag/P25 (Photo) sample and the Ag/TiO_2 (chem) sample were also synthesized and their TEM images could be found in Figs. S2b and c, respectively, in the Supplementary material. Very fine Ag nanoparticles could be observed on P25 TiO_2 nanoparticles with irregular shapes (Fig. S2b), while Ag nanoparticles were found to exist on both {0 0 1} and {1 0 1} facets of our TiO_2 nanocrystals with co-exposed {0 0 1}/{1 0 1} facets for the Ag/TiO_2 (chem) sample (Fig. S2c).

3.2. Optical properties of TiO_2 nanocrystals with co-exposed {0 0 1}/{1 0 1} facets and silver modification on {1 0 1} facets

The optical property of TiO_2 nanocrystals with co-exposed {0 0 1}/{1 0 1} facets and silver modification on {1 0 1} facets was investigated by measuring their diffuse reflectance spectrum. From the reflectance data, the optical absorbance could be approximated by the Kubelka–Munk function, as given by Eq. (1):

$$F(R) = \frac{(1-R)^2}{2R} \quad (1)$$

where R is the diffuse reflectance [48]. Fig. 4 shows the light absorbance (in term of Kubelka–Munk equivalent absorbance units) of the Ag/TiO_2 (photo) sample, compared with that of TiO_2 nanocrystals with co-exposed {0 0 1}/{1 0 1} facets and commercially available Degussa P25 TiO_2 nanoparticles. Degussa P25 TiO_2 nanoparticles are widely used as a model TiO_2 with high photocatalytic performance in the photocatalysis research. As expected, P25 TiO_2 nanoparticles demonstrated their characteristic spectrum with the fundamental absorbance stopping edge at ~400 nm, so its light absorbance was mainly limited in the UV light region. TiO_2 nanocrystals with co-exposed {0 0 1}/{1 0 1} facets, however, demonstrated a moderate light absorption capability from 400 to 500 nm. This observation may be attributed to their nano-size, which largely increased their {0 0 1} surface/bulk ratio. As demonstrated by Ariga et al. [49], a surface state-mediated visible-light activity could occur on nanostructured TiO_2 {0 0 1} facets. With Ag

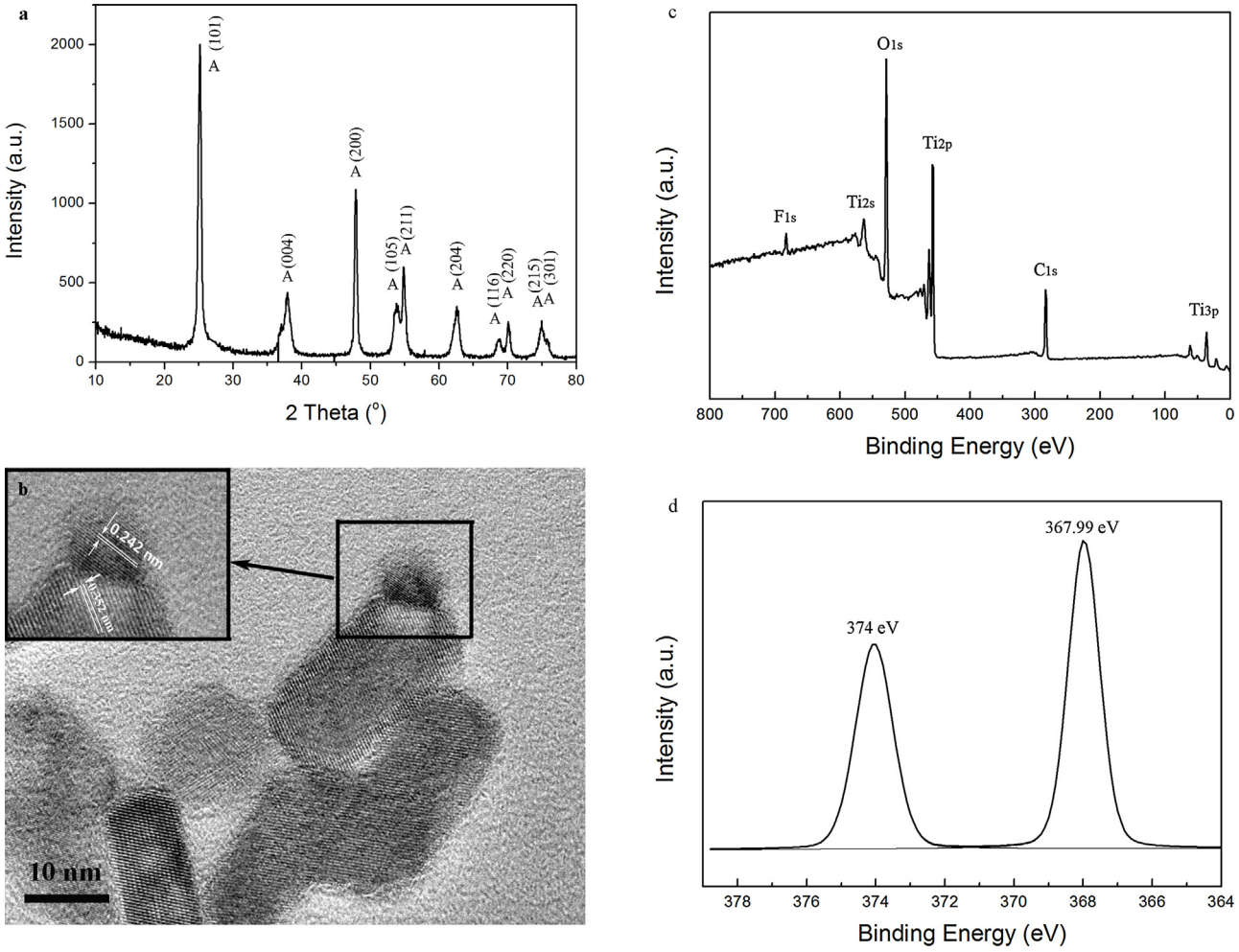

Fig. 3. (a) XRD pattern, (b) HRTEM image, (c) XPS survey spectrum, and (d) High resolution XPS scan spectrum over Ag 3d region of TiO_2 nanocrystals with co-exposed {0 0 1}/{1 0 1} facets and silver modification on {1 0 1} facets.

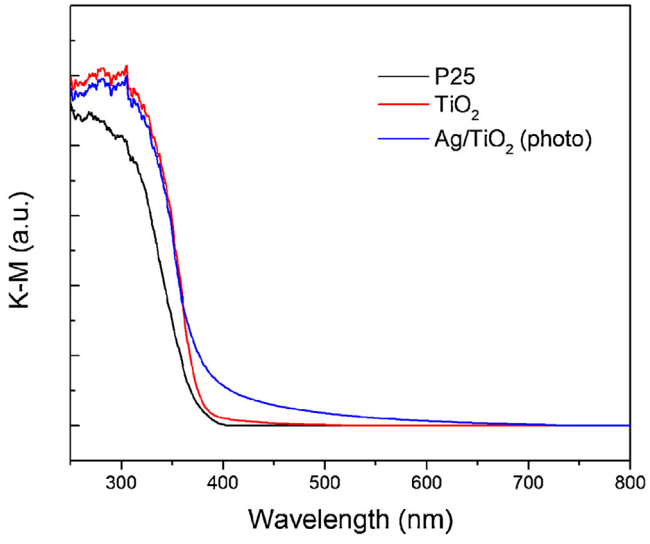

Fig. 4. Light absorbance curves of Degussa P25 TiO_2 nanoparticles (black line), TiO_2 nanocrystals with co-exposed {0 0 1}/{1 0 1} facets (red line), and the Ag/TiO_2 (photo) sample (blue line).

modification, the Ag/TiO_2 (photo) sample demonstrated a largely enhanced visible light absorption capability from 400 to 700 nm, which could be attributed to the enhancement by the localized surface plasmon resonance (LSPR) effect of silver nanoparticles in the visible light region [50,51]. The Ag/TiO_2 (chem) sample had an almost identical light absorbance curve as that of the Ag/TiO_2 (photo) sample due to their same Ag content. It was not included in Fig. 4 for the clarity of the image.

3.3. *Photocatalytic aqueous nitrate reduction performance of TiO_2 nanocrystals with co-exposed {0 0 1}/{1 0 1} facets and silver modification on {1 0 1} facets*

In recent years, the photocatalytic denitrification had been developed and proved to be a promising approach in controlling the concentration of nitrate in water [52–54]. However, most of these researches were conducted under UV illumination, which largely limits their solar efficiency. Furthermore, the most reported aqueous nitrate removal rates were not high and large parts of their reduction products were NO_2^- and NH_4^+, which are toxic and require further treatments [55–58]. Thus, aqueous nitrate was chosen in this study to examine the photocatalytic reduction capability of our sample under a simulated solar illumination. Fig. 5a shows the decrease curves of aqueous nitrate concentration treated by TiO_2 nanocrystals with co-exposed {0 0 1}/{1 0 1} facets w/o silver modification on {1 0 1} facets under a simulated solar illumination from a 300 W xenon lamp, respectively. Without Ag modification, the aqueous nitrate concentration only dropped from ~100 mg/L to ~82.7 mg/L after 2 h treatment by TiO_2 nanocrystals with co-

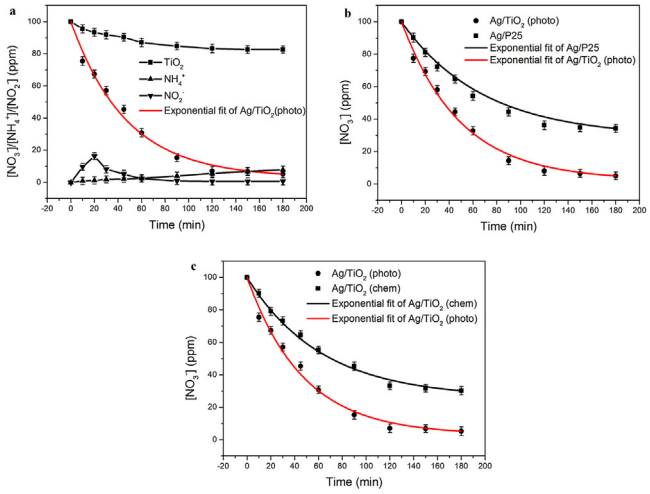

Fig. 5. (a) The decrease curves of aqueous nitrate concentration treated by TiO_2 nanocrystals with co-exposed {0 0 1}/{1 0 1} facets with silver modification on {1 0 1} facets under a simulated solar illumination (■: [NO_3^-] by TiO_2 nanocrystals with co-exposed {0 0 1}/{1 0 1} facets, ●: [NO_3^-] by the Ag/TiO_2 (photo) sample, ▲: [NH_4^+] by the Ag/TiO_2 (photo) sample, and ▼: [NO_2^-] by the Ag/TiO_2 (photo) sample). (b) The decrease curves of aqueous nitrate concentration treated by the Ag/P25 (Photo) sample (■) and by the Ag/TiO_2 (photo) sample (●). (c) The decrease curves of aqueous nitrate concentration treated by the Ag/TiO_2 (chem) sample (■) and by the Ag/TiO_2 (photo) sample (●). (Note: All photocatalytic aqueous nitrate reduction curves were fitted with the first-order exponential decay curves).

exposed {0 0 1}/{1 0 1} facets, which could be mainly attributed to the adsorption of nitrate on the surface of these TiO_2 nanocrystals. This observation was consistent to previous reports that pure TiO_2 hardly had the photocatalytic reduction activity to aqueous nitrate [59–61]. With Ag modification on {1 0 1} facet, however, the Ag/TiO_2 (photo) sample demonstrated a superior photocatalytic reduction performance on aqueous nitrate. After 2 h treatment, the aqueous nitrate concentration dropped from ~100 mg/L to only ~5.3 mg/L, representing a removal ratio of ~95%. During the photocatalytic treatment process, the concentration of NO_2^- increased initially within the first 20 min and then gradually decreased, while the concentration of NH_4^+ gradually increased. After 2 h treatment, only small amounts of NO_2^- (0.67 mg/L, ~0.67% of the initial aqueous NO_3^- concentration) and NH_4^+ (7.8 mg/L, ~7.8% of the initial aqueous NO_3^- concentration) were found in the treated solution, which was far less than some previous reports [55–58]. This observation confirmed the photocatalytic reduction of NO_3^- by the Ag/TiO_2 (photo) sample and demonstrated that the major NO_3^- reduction product was the desirable N_2 with a high N_2 product selectivity of ~91%. The superior photocatalytic reduction performance on aqueous nitrate of the Ag/TiO_2 (photo) sample suggested that Ag modification on TiO_2 was critical to the photocatalytic reduction of aqueous nitrate, which was consistent with previous reports that the loading of metals on TiO_2 was necessary for the photocatalytic reduction of aqueous nitrate [59–61].

Fig. 5b shows the decrease curves of aqueous nitrate concentration treated by the Ag/TiO_2 (photo) sample and the Ag/P25 (photo) sample under the simulated solar illumination from a 300 W xenon lamp, respectively. For both samples, the silver modification was introduced by our modified photo-deposition process and the Ag:Ti molar ratio was ~1:200. When the Ag/P25 (photo) sample was used, the aqueous nitrate concentration dropped from ~100 mg/L to ~34.2 mg/L after 2 h treatment, representing a removal ratio of ~66%, which was much less than that by the Ag/TiO_2 (photo) sample under the same reaction conditions (~95%). A first-order exponential decay of aqueous nitrate concentration was observed for both samples, which could be fitted to Eq. (2):

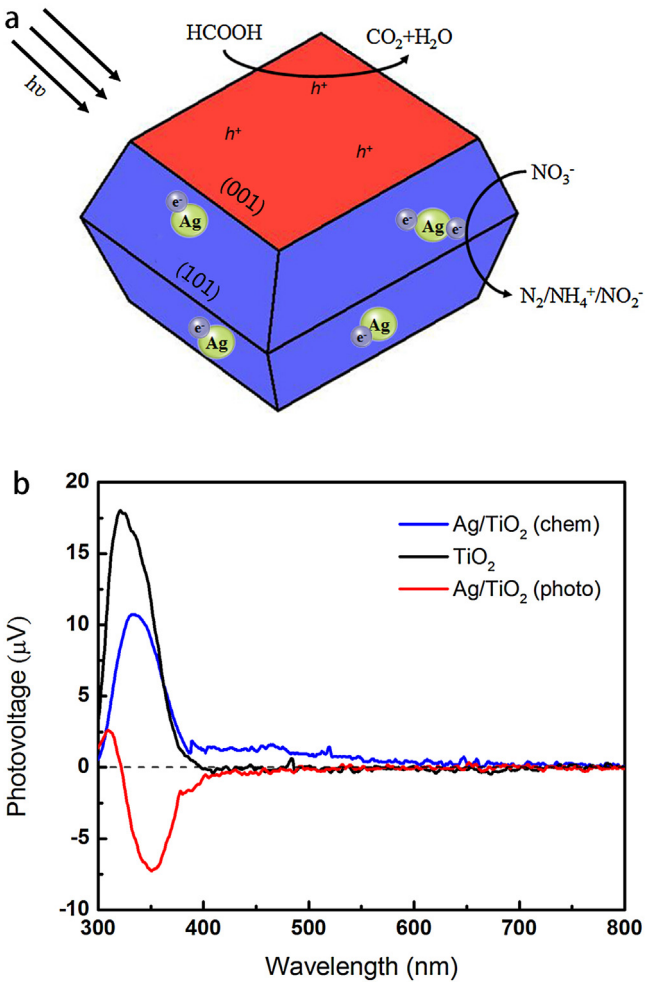

Fig. 6. (a) Schematic illustration of the photocatalytic reduction process of aqueous nitrate by the Ag/TiO_2 (photo) sample. (b) The SPS measurement results of TiO_2 nanocrystal with co-exposed {0 0 1}/{1 0 1} facets (black line), the Ag/TiO_2 (chem) sample (blue line), and the Ag/TiO_2 (photo) sample (red line).

$$C_R = ae^{-bt} \quad (2)$$

where C_R is the residue aqueous nitrate concentration, t is the visible light illumination time, and a and b are the first-order exponential fitting constants. This kind of first-order exponential fitting had been observed for various photocatalytic reactions [62–65]. Constant b, the decay rate, could be used to compare the photocatalytic reduction efficiency of different samples. The decay rate of the Ag/P25 (photo) sample was determined at 0.0063, while that of the Ag/TiO_2 (photo) sample was determined at ~0.0178, representing a ~282% increase. These results demonstrated that TiO_2 nanocrystals with co-exposed {0 0 1}/{1 0 1} facets and silver modification on {1 0 1} facets had a much better photocatalytic reduction performance on aqueous nitrate than Degussa P25 TiO_2 nanoparticles with the same amount of silver modification. Thus, this observation suggested that the creation of co-exposed {0 0 1}/{1 0 1} facets could largely enhance the photocatalytic performance of TiO_2 photocatalyst due to their better charge carrier separation and subsequent separation of oxidation and reduction sites in space [24–29].

Fig. 5c shows the decrease curves of aqueous nitrate concentration treated by the Ag/TiO_2 (photo) sample and the Ag/TiO_2 (chem) sample under the simulated solar illumination from a 300 W

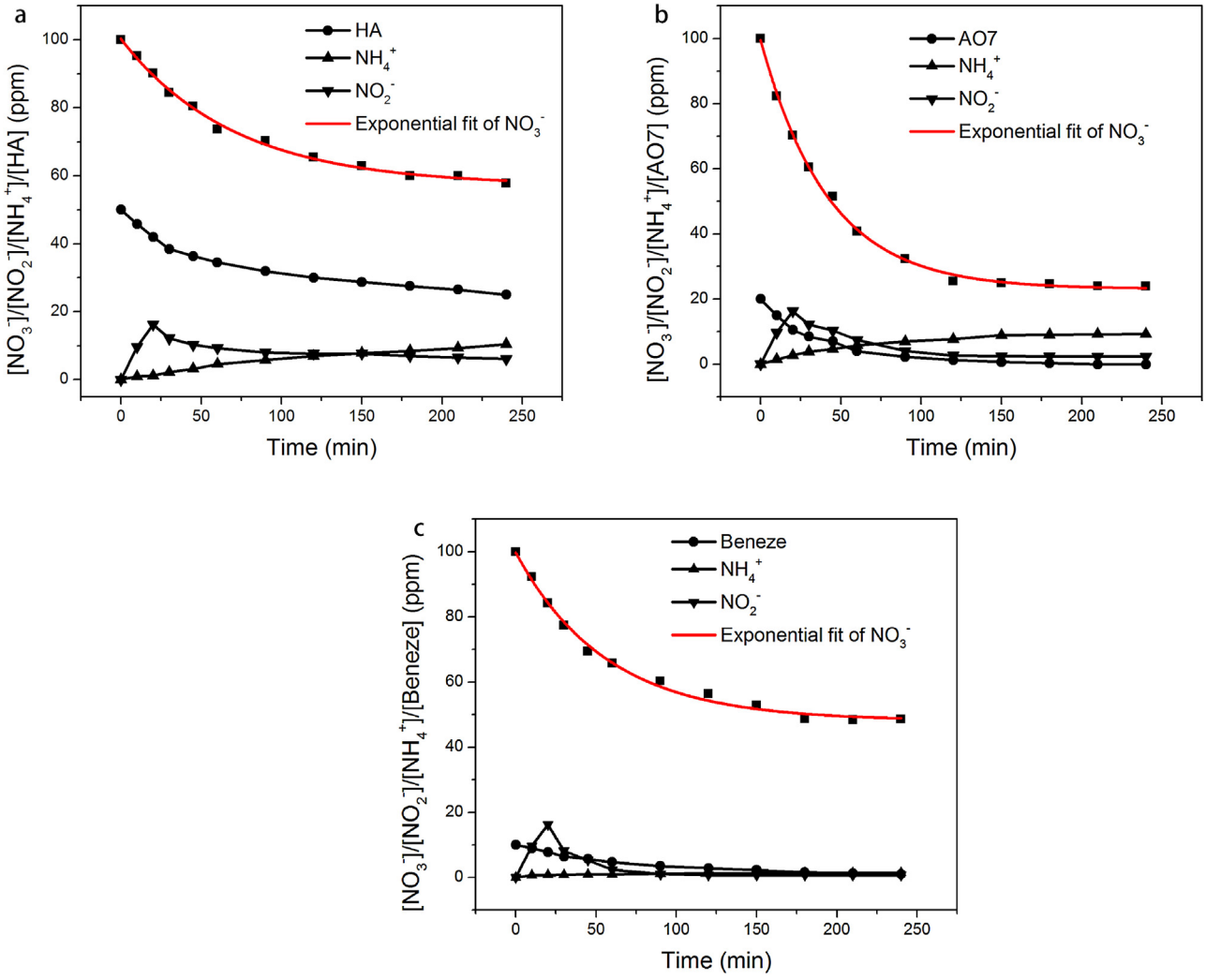

Fig. 7. The decrease curves of aqueous nitrate concentration treated by TiO_2 nanocrystals with co-exposed {0 0 1}/{1 0 1} facets with silver modification on {1 0 1} facets under a simulated solar illumination: (a) with the co-existence of humic acids (■: [NO_3^-], ●: [HA], ▲: [NH_4^+], and ▼: [NO_2^-]), (b) with the co-existence of AO7 dye (■: [NO_3^-], ●: [AO7], ▲: [NH_4^+], and ▼: [NO_2^-]), and (c) with the co-existence of benzene (■: [NO_3^-], ●: [benzene], ▲: [NH_4^+], and ▼: [NO_2^-]). (Note: All photocatalytic aqueous nitrate reduction curves were fitted with the first-order exponential decay curves).

xenon lamp, respectively. For both samples, the same amount of silver modification (Ag: Ti molar ratio at ~1:200) was deposited on TiO_2 nanocrystal with co-exposed {0 0 1}/{1 0 1} facets, and they had almost identical light absorbance behavior. The silver modification was introduced by either our modified photo-deposition process or the chemical reduction method, respectively. When the Ag/TiO_2 (chem) sample was used, the aqueous nitrate concentration dropped from ~100 mg/L to ~30.2 mg/L after 2 h treatment, representing a removal ratio of ~70%, which was much less than that by the Ag/TiO_2 (photo) sample under the same reaction conditions (~95%). The decay rate of the Ag/TiO_2 (chem) sample was determined at ~0.0070, while that of the Ag/TiO_2 (photo) sample was determined at ~0.0178, representing a ~254% increase. These results demonstrated that TiO_2 nanocrystals with co-exposed {0 0 1}/{1 0 1} facets and silver modification on {1 0 1} facets had a much better photocatalytic reduction performance on aqueous nitrate than TiO_2 nanocrystals with co-exposed {0 0 1}/{1 0 1} facets and silver modification randomly deposited on both {0 0 1} and {1 0 1} facets. Thus, this observation suggested that the selective deposition of Ag nanoparticles on {1 0 1} facet had a better charge carrier separation effect and subsequent separation of oxidation and reduction sites than the random deposition of Ag nanoparticles on both {0 0 1} and {1 0 1} facets because it could combine the advantages from both the crystal facet effect and noble metal modification to enrich the presence of photogenerated electrons onto the surface of TiO_2 for the enhanced photocatalytic reduction activity, while the deposition of Ag nanoparticles on {0 0 1} facets may cause photogenerated electrons and holes to recombine on {0 0 1} facets.

3.4. Enhancement mechanism of photocatalytic reduction of aqueous nitrate by TiO_2 nanocrystals with co-exposed {0 0 1}/{1 0 1} facets and silver modification on {1 0 1} facets

Fig. 6a schematically demonstrates the photocatalytic reduction process of aqueous nitrate by TiO_2 nanocrystals with co-exposed {0 0 1}/{1 0 1} facets and silver modification on {1 0 1} facets. Due to the synergistic effect of surface energy differences between {0 0 1}/{1 0 1} facets and the selective deposition of silver nanoparticles on {1 0 1} facets, the separation of photogenerated carriers was largely enhanced under illumination. Photogenerated holes were driven to {0 0 1} facets to create oxidation facets and react with the sacrifice agent HCOOH, while photogenerated electrons were driven to {1 0 1} facets to make them reductive and reduce nitrate. The photocatalytic reduction of aqueous nitrate took place through several parallel and consecutive reaction steps, leading to

the formation of various products as N_2, NO_2^-, and NH_4^+ [66–68]. Both the photo-oxidation reaction (consuming the photoinduced holes) and photo-reduction reaction (consuming the photoinduced electrons) are important steps and could affect each other in photocatalytic reactions. Thus, the creation of co-exposed {0 0 1}/{1 0 1} facets for different reaction processes is favorable for the photocatalytic reduction of aqueous nitrate, which could efficiently reduce side reactions.

The surface photovoltage spectrum (SPS) measurements were conducted to further examine the photo-induced carrier separation and transfer behaviors in our samples. When photogenerated charge carriers are separated in space, a photovoltage will arise. In a semiconducting material, the formation of a surface photovoltage (SPV) signal is determined by the fundamental properties of its light absorption and the transport of excess carriers [69–73]. Fig. 6b compares the SPS measurement results of TiO_2 nanocrystal with co-exposed {0 0 1}/{1 0 1} facets, the Ag/TiO_2 (chem) sample, and the Ag/TiO_2 (photo) sample. For TiO_2 nanocrystal with co-exposed {0 0 1}/{1 0 1} facets, a positive SPV signal was observed, which indicated that the number of photogenerated holes that transferred to the sample surface was over the number of photogenerated electrons that transferred to the sample surface [74]. Thus, the net charge on the sample's surface was positive. For the Ag/TiO_2 (chem) sample, it also had a positive SPV signal till ~600 nm, but the signal intensity was lower than that of the sample without silver modification in most of the UV region. It is well known that the introduction of a small amount of noble metal modification onto the surface of photocatalysts could largely enhance the oriented migration of photogenerated electrons. Compared with the sample without silver modification, the decreased SPV signal observed here with silver modification suggested that more photogenerated electrons moved to the surface of TiO_2 nanocrystals, which enhanced its photocatalytic reduction capability as demonstrated in its better photocatalytic reduction of aqueous nitrate performance (see Fig. 5). Ag nanoparticles, especially those on {0 0 1} facets, could also form more recombination centers, which subsequently resulted in higher recombination rate of electrons and holes and decreased the SPV signal. When the same amount of silver modification was selectively deposited only on {1 0 1} facets, a negative SPV signal was observed for the Ag/TiO_2 (photo) sample. The synergistic effect of crystal facet engineering and the selective deposition of silver nanoparticles on {1 0 1} facets further enhanced the accumulation of photogenerated electrons on {1 0 1} facets. Thus, the number of photogenerated electrons that transferred to the sample surface was over the number of photogenerated holes that transferred to the sample surface, which resulted in a negative charge on the surface of the Ag/TiO_2 (photo) sample. That is the reason for the Ag/TiO_2 (photo) sample to have a strong photocatalytic reduction capability as demonstrated in its best photocatalytic reduction of aqueous nitrate performance among all the samples we examined.

3.5. Photocatalytic reduction of aqueous nitrate with the co-existence of organic pollutants in water by TiO_2 nanocrystals with co-exposed {0 0 1}/{1 0 1} facets and silver modification on {1 0 1} facets

In ground water, nitrate is usually present with the co-existence of various organic pollutants from both natural occurrences and anthropogenic activities [75,76]. Thus, it is of interests to examine if the Ag/TiO_2 (photo) sample could exhibit the multifunctional capability to effectively remove both nitrate and organic pollutants from water simultaneously. In this series of experiments, three commonly found organic pollutants of humic acids, AO7, and benzene were used, which represented the natural organics, organic dyes, and petroleum hydrocarbons, respectively, and had been explored as sacrificial agents in various photocatalytic studies [75–77]. Fig. 7 shows the decrease curves of aqueous nitrate concentration treated by the Ag/TiO_2 (photo) sample with the co-existence of humic acid, AO7 dye, and benzene under the simulated solar illumination from a 300 W xenon lamp, respectively. It demonstrated clearly that nitrate could be effectively removed with the relatively low by-product production of NO_2^- and NH_4^+, while these organic pollutants could also be removed effectively. Thus, the Ag/TiO_2 (photo) sample had the potential to photocatalytically remove both nitrate and organic pollutants in water under solar illumination simultaneously.

4. Conclusions

In summary, a modified photo-deposition process was developed which allowed the selective deposition of silver nanoparticles on {1 0 1} facets of TiO_2 nanocrystals with co-exposed {0 0 1}/{1 0 1} facets. The synergistic effect of crystal facet engineering and the selective deposition of silver nanoparticles on {1 0 1} facets largely enhanced the accumulation of photogenerated electrons onto {1 0 1} facets, which resulted in a negative charge on the surface of the Ag/TiO_2 (photo) sample and subsequently introduced a strong photocatalytic reduction capability to the sample. Under a simulated solar illumination, the removal ratio of aqueous nitrate reached ~95%, and most of the reduction product was the desirable N_2. These TiO_2 nanocrystal with co-exposed {0 0 1}/{1 0 1} facets and silver modification on {1 0 1} facets also demonstrated a multifunctional capability to effectively remove both nitrate and organic pollutants from water simultaneously. This material design strategy could be readily applied to the modification of noble metal nanoparticles on a variety of photocatalysts with exposed facets to create photocatalysts with strong photocatalytic reduction capabilities for a broad range of environmental application.

Acknowledgments

The authors would like to thank Prof. Dejun Wang and Mr. Linqi Shi of College of Chemistry, Jilin University for the experimental assistance and useful discussion on the surface photovoltage spectrum measurement. This study was supported by the National Natural Science Foundation of China (Grant No. 51102246), the Knowledge Innovation Program of Institute of Metal Research, Chinese Academy of Sciences (Grant No. Y0N5A111A1), the Youth Innovation Promotion Association, Chinese Academy of Sciences (Grant No. Y2N5711171), the Scientific Research Foundation for the Returned Overseas Chinese Scholars, State Education Ministry, PR China, and the Basic Science Innovation Program of Shenyang National Laboratory for Materials Science (Grant No. Y4N56R1161).

Appendix A. Supplementary data

Supplementary data associated with this article can be found, in the online version, at http://dx.doi.org/10.1016/j.apcatb.2015.09.005.

References

[1] B. O'Regan, M. GrGtzel, Nature 353 (1991) 737–740.
[2] A.L. Linsebigler, G. Lu, J.T. Yates, Chem. Rev. 95 (1995) 735–758.
[3] G.K. Mor, K. Shankar, M. Paulose, Nano Lett. 6 (2) (2006) 215–218.
[4] G. Roland, Water Sci. Technol. 35 (1997) 137–138.
[5] I.L. Marta, Appl. Catal. B 23 (1999) 89–114.
[6] C. Minero, E. Pelizzetti, J. Malato, J. Blanco, Solar Energy 56 (1996) 421–428.
[7] H.G. Yang, C.H. Sun, S.Z. Qiao, J. Zou, G. Liu, S.C. Smith, H.M. Cheng, G.Q. Lu, Nature 453 (2008) 638–641.
[8] H.G. Yang, G. Liu, S.Z. Qiao, C.H. Sun, Y.G. Jin, S.C. Smith, J. Zou, H.M. Cheng, G.Q. Lu, J. Am. Chem. Soc. 131 (2009) 4078–4083.
[9] J. Jiang, K. Zhao, X.Y. Xiao, L.Z. Zhang, J. Am. Chem. Soc. 134 (2012) 4473–4476.

[10] H. Liu, M. Luo, J.C. Hu, T.F. Zhou, R. Chen, J.L. Li, Appl. Catal. B 140 (2013) 141–150.
[11] Y. Zhou, Z.P. Tian, Z.Y. Zhao, Q. Liu, J.H. Kou, X.Y. Chen, J. Gao, S.C. Yan, Z.G. Zou, ACS Appl. Mater. Interfaces 3 (2011) 3594–3601.
[12] H. Zhao, W.Y. Yin, M.Y. Zhao, Y.Z. Song, H.Q. Yang, Appl. Catal. B 130 (2013) 178–186.
[13] S.D. Sun, X.P. Song, Y.X. Sun, D.C. Deng, Z.M. Yang, Catal. Sci. Technol. 2 (2012) 925–930.
[14] T. Tachikawa, S. Yamashita, T. Majima, J. Am. Chem. Soc. 133 (2011) 7197–7204.
[15] J. Pan, G. Liu, G.Q. Lu, H.M. Cheng, Angew. Chem. 50 (2011) 2133–2137.
[16] T.R. Gordon, M. Cargnello, T. Paik, F. Mangolini, R.T. Weber, P. Fornasiero, C.B. Murray, J. Am. Chem. Soc. 134 (2012) 6751–6761.
[17] J.A. Zhu, S.H. Wang, Z.F. Bian, S.H. Xie, C.L. Cai, J.G. Wang, H.G. Yang, H.X. Li, CrystEngComm 12 (2010) 2219–2224.
[18] W.J. Shi, W.Y. Yang, Q. Li, S.A. Gao, P.J. Shang1, J.K. Shang, Nanoscale Res. Lett. 7 (2012) 590.
[19] Q.J. Xiang, K.L. Lv, J.G. Yu, Appl. Catal. B 96 (2010) 557–564.
[20] Z.K. Zheng, B.B. Huang, J.B. Lu, X.Y. Qin, X.Y. Zhang, Y. Dai, J. Chem. Eur. 17 (2011) 15032–15038.
[21] M. Liu, L.Y. Piao, L. Zhao, S.T. Ju, Z.J. Yan, T. He, C.L. Zhou, W.J. Wang, Chem. Commun. 46 (2010) 1664–1666.
[22] Z.F. Jiang, X.M. Lv, D.L. Jiang, J.M. Xie, D.J. Mao, J. Mater. Chem. A 1 (2013) 14963.
[23] R. Hengerer, L. Kavan, P. Krtil, M.Z. Gratzel, Electrochem. Soc. 147 (2000) 1467.
[24] M. D'Arienzo, J. Carbajo, A. Bahamonde, M. Crippa, S. Polizzi, R. Scotti, L. Wahba, F. Morazzoni, J. Am. Chem. Soc. 133 (2011) 17652–17661.
[25] M.K. Nowotny, L.R. Sheppard, T. Bak, J. Nowotny, J. Phys. Chem. C 112 (2008) 5275–5300.
[26] H.Z. Cheng, A. Selloni, Phys. Rev. B 79 (2009) 92101-1–92101-4.
[27] A. Selloni, Nat. Mater. 7 (2008) 613–615.
[28] N. Roy, Y. Sohn, D. Pradhan, ACS Nano 7 (2013) 2532–2540.
[29] C. Liu, X. Han, S. Xie, Q. Kuang, X. Wang, M. Jin, Z. Xie, L. Zheng, J. Chem. Asian 8 (2013) 282–289.
[30] H.B. Michaelson, J. Appl. Phys. 48 (1977) 4729–4733.
[31] Y.C. Lu, Y.H. Lin, T.F. Xie, L.P. Chen, S.S. Yi, D.J. Wang, ACS Appl. Mater. Interfaces 5 (2013) 4017–4020.
[32] N.S. Norberg, D.R. Gamelin, J. Phys. Chem. B 109 (2005) 20810–20816.
[33] H.M. Fan, T.F. Jiang, H.Y. Li, D.J. Wang, L.L. Wang, J.L. Zhai, D.Q. He, P. Wang, T.F. Xie, J. Phys. Chem. C 116 (2012) 2425–2430.
[34] W.E. Fameth, R.S. McLean, J.D. Bolt, E. Dokou, M.A. Barteau, Langmuir 15 (1999) 8569.
[35] W.E. Farneth, P.M.A. Hotsenpiller, J.D. Bolt, J.B. Lowekamp, G.S. Rohrer, J. Am. Chem. Soc. 1 (1998) 216.
[36] Z.Q. He, Q.L. Cai, M. Wu, Y.Q. Shi, H.Y. Fang, L.D. Li, J.C. Chen, J.M. Chen, S. Song, Ind. Eng. Chem. Res. 52 (2013) 9556–9565.
[37] W. Yan, S.M. Mahurin, Z. Pan, S.H. Overbury, S. Dai, J. Am. Chem. Soc. 127 (2005) 10480–10481.
[38] M. Haruta, S. Tsubota, T. Kobayashi, H. Kageyama, M.J. Genet, B. Delmon, J. Catal. 144 (1993) 175–192.
[39] M. Manzoli, A. Chiorino, F. Boccuzzi, Appl. Catal. B 57 (2005) 201–209.
[40] J. Choi, H. Park, M.R. Hoffmann, J. Phys. Chem. C 114 (2009) 783–792.
[41] M.A. Khan, O.Y. Bong, J. Hydro Energy 33 (2008) 5345–5351.
[42] M.A. Behnajady, N. Modirshahla, M. Shokri, et al., Global NEST 10 (2008) 1–7.
[43] L.J. Guillette, T.M. Edwards, Integr. Comp. Biol. 45 (2005) 19–27.
[44] H.J. Hamlin, B.C. Moore, T.M. Edwards, I.L.V. Larkin, A. Boggs, W.J. High, K.L. Main, L.J. Guillette, Aquaculture 281 (2008) 118–125.
[45] H.J. Hamlin, Aquaculture 253 (2006) 688–693.
[46] Y.H. Liu, D.J. Wang, Q.D. Zhang, M. Yang, Q.L. Zhang, J. Phys. Chem. B 108 (2004) 3202–3206.
[47] J.C. Fuggle, E.K. ällne, L.M. Watson, D.J. Fabian, Phys. Rev. B. 16 (1997) 750–761.
[48] J. Tauc, R. Grigorovici, A. Vancu, Phys. Status Solidi B 15 (1966) 627–637.
[49] H. Ariga, T. Taniike, H. Morikawa, M. Tada, B.K. Min, K. Watanabe, Y. Matsumoto, S. Ikeda, K. Saiki, Y. Iwasawa, J. Am. Chem. Soc. 131 (2009) 14670–14672.
[50] S. Zhu, S. Liang, Q. Gu, L. Xie, J. Wang, Z. Ding, P. Liu, Appl. Catal. B 119–120 (2012) 146–155.
[51] X. Chen, Z. Zheng, X. Ke, E. Jaatinen, T. Xie, D. Wang, C. Guo, J. Zhao, H. Zhu, Green Chem. 12 (2010) 414–419.
[52] A. Kudo, K. Domen, H. Maruya, T. Ohnishi, J. Catal. 135 (1992) 300–303.
[53] B. Bems, F.C. Jentoft, R. Schlogl, Appl. Catal. B 20 (1999) 155–163.
[54] K.T. Ranjit, B. Viswannathan, J. Photochem. Photobiol. A 107 (1997) 215–220.
[55] J.A. Anderson, Catal Today 181 (2012) 171–176.
[56] H. Kominami, H. Gekko, K. Hashimoto, Phys. Chem. Chem. Phys. 12 (2010) 15423–15427.
[57] A. Pandikumar, S. Manonmani, R. Ramaraj, Catal. Sci. Technol. 2 (2012) 345–353.
[58] K. Doudricka, T. Yanga, K. Hristovskia, P. Westerhoffa, Appl. Catal. B 136–137 (2013) 40–47.
[59] S. Rengaraj, X.Z. Li, Chemosphere 66 (2007) 930.
[60] F. Zhang, R. Jin, J. Chen, C. Shao, W. Gao, L. Li, N.J. Guan, J. Catal. 223 (2005) 424.
[61] R. Jin, W. Gao, J. Chen, H. Zeng, F. Zhang, Z. Liu, N.J. Guan, J. Photochem. Photobiol. A 116 (2004) 585.
[62] H. Liu, S.A. Cheng, J.Q. Zhang, C.A. Cao, S.K. Zhang, Chemosphere 38 (1999) 283–292.
[63] D.D. Dionysiou, A.P. Khodadoust, A.M. Kern, M.T. Suidan, I. Baudin, J.M. Laine, Appl. Catal. B 24 (2000) 139–155.
[64] X. Domenech, J. Peral, Chemosphere 38 (1999) 1265–1271.
[65] W.H. Leng, H. Liu, S.A. Cheng, J. Zhang, C. Cao, J. Photochem. Photobiol. A 131 (2000) 125–132.
[66] H. Kominami, T. Nakaseko, Y. Shimada, A. Furusho, H. Inoue, S. Murakami, Y. Kera, B. Ohtani, Chem. Commun. 23 (2005) 2933–2935.
[67] H. Kominami, A. Furusho, S. Murakami, H. Inoue, Y. Kera, B. Ohtani, Catal. Lett. 76 (2001) 31.
[68] A. Kudo, K. Domen, K.I. Maruya, T. Onishi, J. Catal. 135 (1992) 300.
[69] L. Kronik, Y. Shapira, Surf. Sci. Rep. 37 (1999) 1.
[70] T.F. Xie, D.J. Wang, L.J. Zhu, C. Wang, T.J. Li, X.Q. Zhou, M. Wang, J. Phys. Chem. B 104 (2000) 8177.
[71] D. Gross, I. Mora-Sero, T. Dittrich, A. Belaidi, C. Mauser, A.J. Houtepen, E. Da Como, A.L. Rogach, J. Feldmann, J. Am. Chem. Soc. 132 (2010) 5981.
[72] F.A. Frame, T.K. Townsend, R.L. Chamousis, E.M. Sabio, T. Dittrich, N.D. Browning, F.E. Osterloh, J. Am. Chem. Soc. 133 (2011) 7264.
[73] J. Zhang, D.J. Wang, T.S. Shi, B.H. Wang, J.Z. Sun, T.J. Li, Thin Solid Films 284 (1996) 596.
[74] V. Duzhko, V.Y. Timoshenko, F. Koch, T. Dittrich, Phys. Rev. B 64 (2001) 1–75204.
[75] B. Bems, F.C. Jentoft, R. SchloÈgl, Appl. Catal. B 20 (1999) 155–163.
[76] L.Y. Li, Z.Y. Xu, F.L. Liu, Y. Shao, J.H. Wang, H.Q. Wan, S.R. Zheng, J. Photochem. Photobiol. A 212 (2010) 113–121.
[77] S.S. Lee, H.W. Bai, Z.Y. Liu, D.D. Sun, Water Res. 47 (2013) 4059–4073.